HighlightRemover: Spatially Valid Pixel Learning for Image Specular Highlight Removal

Ling Zhang
School of Computer Science and Technology, Hubei Key Laboratory of Intelligent Information Processing and Realtime Industrial Systems
Wuhan University of Science and Technology
Wuhan, China
zhling@wust.edu.cn

Yidong Ma
School of Computer Science
Wuhan University
Wuhan, China
yidongma@whu.edu.cn

Zhi Jiang
School of Computer Science
Wuhan University
Wuhan, China
z1203685136@gmail.com

Weilei He
School of Computer Science
Wuhan University
Wuhan, China
weileihe090@whu.edu.cn

Zhongyun Bao
School of Computer Science
Wuhan University
Wuhan, China
tantouxy@163.com

Gang Fu
Department of Computing
Hong Kong Polytechnic University
Hong Kong SAR, China
xyzgfu@gmail.com

Wenju Xu
AMAZON
Palo Alto, USA
xuwenju123@gmail.com

Chunxia Xiao*
School of Computer Science
Wuhan University
Wuhan, China
cxxiao@whu.edu.cn

ABSTRACT

Recently, learning-based methods have made significant progress for image specular highlight removal. However, many of these approaches treat all the image pixels uniformly, overlooking the negative impact of invalid pixels on feature reconstruction. This oversight often leads to undesirable outcomes, such as color distortion or residual highlights. In this paper, we propose a novel image specular highlight removal network called HighlightRNet, which utilizes valid pixels as references to reconstruct the highlight-free image. To achieve this, we introduce a context-aware fusion block (CFBlock) that aggregates information in four directions, effectively capturing global contextual information. Additionally, we introduce a location-aware feature transformation module (LFTModule) to adaptively learn the valid pixels for feature reconstruction, thereby avoiding information errors caused by invalid pixels. With these modules, our method can produce high-quality highlight-free results without color distortion and highlight residual. Furthermore, we develop a multiple light image-capturing system to construct a large-scale highlight dataset called NSH, which exhibits minimal misalignment in image pairs and minimal brightness variation in non-highlight regions. Experimental results on various datasets demonstrate the superiority of our method over state-of-the-art methods, both qualitatively and quantitatively.

CCS CONCEPTS

• **Computing methodologies** → **Computer vision problems**.

KEYWORDS

Image specular highlight removal, contextual information, valid pixels

ACM Reference Format:
Ling Zhang, Yidong Ma, Zhi Jiang, Weilei He, Zhongyun Bao, Gang Fu, Wenju Xu, and Chunxia Xiao. 2024. HighlightRemover: Spatially Valid Pixel Learning for Image Specular Highlight Removal. In *Proceedings of the 32nd ACM International Conference on Multimedia (MM '24), October 28-November 1, 2024, Melbourne, VIC, Australia.* ACM, New York, NY, USA, 9 pages. https://doi.org/10.1145/3664647.3681434

1 INTRODUCTION

Specular highlights are natural occurrences when light strikes an object with smooth surface. However, the presence of continuous or discontinuous spots in specular highlight regions often leads to poor visibility and incoherent diffuse regions in images. This phenomenon significantly increases the complexity and difficulty of various vision tasks, including object detection [5, 15], semantic segmentation [3, 4], object tracking [8], image segmentation [14], and so on. Therefore, effectively removing specular highlights from

*Corresponding author.

MM '24, October 28-November 1, 2024, Melbourne, VIC, Australia

ACM ISBN 979-8-4007-0686-8/24/10.
https://doi.org/10.1145/3664647.3681434

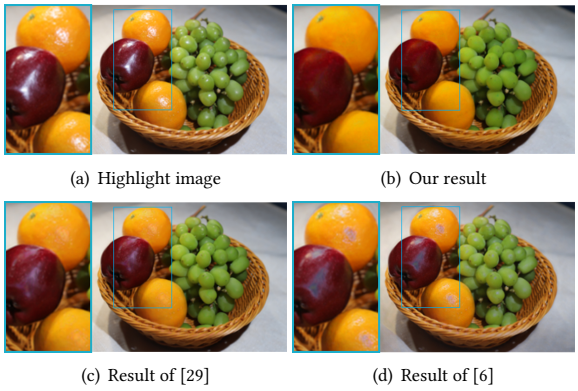

(a) Highlight image (b) Our result

(c) Result of [29] (d) Result of [6]

Figure 1: Image specular highlight removal. With consistent feature manipulations, results of [29] and [6] may cause color distortion or highlight residual. In contrast, our method can produce more desirable result by utilizing valid pixels.

images and recovering clear, highlight-free images is both important and challenging.

Existing image specular highlight removal methods fall into two groups. Traditional methods [14, 26, 32, 33] leverage various constraints or assumptions to remove highlights from images but often demonstrate limited effectiveness. Recently, numerous learning-based specular highlight removal methods have been developed [6, 11, 12, 29, 34]. They dig into the mapping relationship between highlight images and non-highlight images, aiming for enhanced performance. However, most of these methods uniformly process all pixels in the image, creating potential problems such as convolution of invalid pixels or deviation calculation of features. The main reason is that, the highlight regions with strong light spots are corrupted regions, and pixels in these region are invalid pixels for specular highlight removal. Simply mapping the features via consistent processing contains convolution of invalid pixels, resulting in mean and variance shifts in normalized features. It can result in invalid or biased recovery in highlight regions, leading to unsatisfactory results with highlight residual or color distortion, as shown in Figure 1(c, d).

Moreover, the dataset has a crucial impact on the performance of learning-based models. Currently, there are only three benchmark datasets publicly available for specular highlight removal. However, these datasets still have quality defects. For example, SHIQ [6] and SSHR [7] are synthesized datasets. But the synthetic images still exhibit some statistical feature differences from the real images. On the other hand, PSD [29] is a real-world dataset, while the image pairs in this dataset suffer from obvious misalignment and brightness inconsistency in non-highlight regions.

To address the above challenges, we propose a novel image specular highlight removal network called HighlightRNet, which utilizes valid pixels in the image to reconstruct the highlight-free image. Figure 2 illustrates the framework of the proposed HighlightRNet, which is an encoder-decoder structure with a discriminator. Specifically, we introduce a context-aware fusion block (CFBlock) in the bottleneck module, which learns global contextual information in four directions and passes feature information from each pixel to the others. After several convolutions, the highlight region is gradually recovered, resulting in a distinct appearance from the original image. To this end, we propose a location-aware feature transformation module (LFTModule). Based on the spatial relationship of features, this module learns a spatial saliency map to demonstrate which are the valid pixels for specular highlight removal task. Thus, we can redecode the features using the valid pixels as references, avoiding information error caused by invalid pixels and promoting high-quality highlight-free results without color distortion and highlight residual, as shown in Figure 1(b).

Additionally, we construct a new large-scale real-world highlight dataset for specular highlight removal. To obtain high-quality highlight image pairs, we build a simple yet effective image-capturing system with multiple light sources. This multiple light source combination mechanism effectively avoids problems such as misalignment between image pair and inconsistent brightness in non-highlight regions. Our image-capturing system is portable and suitable for indoor and outdoor use. Experimental results and evaluations demonstrate the superiority of our dataset and the efficacy of the proposed method.

To sum up, our contributions are summarized as follows:

- We propose a network called HighlightRNet to remove specular highlights in the image, which can recover a high-quality highlight removal results without color distortion and highlight residual.
- We introduce a context-aware fusion block to learn global contextual information and a spatial feature redecoding module to reconstruct the image features using valid pixels as references.
- We construct a real-world highlight dataset without misalignment between image pair and with consistent brightness in non-highlight regions.

2 RELATED WORK

Traditional methods for image specular highlight removal often rely on additional prior knowledge [10, 19, 28, 31]. Shafer *et al.* [23] introduced a method to analyze standard color image to estimate the amount of interface (specular) and body (diffuse) reflection at each pixel. Klinker *et al.* [17] used the difference between the object color and highlight color to separate each pixel into a matte component and a highlight component. Shen *et al.* [24] separated reflections in a color image based on the error analysis of chromaticity and the appropriate selection of body color for each pixel. Yang and Tang [32] formulated the highlight removal problem as an iterative bilateral filtering process. The method proposed by Kim *et al.* [14] was based on the observation that the dark channel usually provides an approximate highlight-free image. Shen and Zheng [25] considered color space to analyze the distribution of the diffuse and specular components and used this information for separation. Akashi [1] proposed a model-driven approach to improve the lighting normalization of face images. Zhang *et al.* [35] formulated highlight detection as a Non-negative Matrix Factorization (NMF) problem.

With the development of deep learning, numerous learning-based methods have been proposed for image specular highlight removal, showing promising results using annotated training data. Lin *et al.* [18] proposed a fully-convolutional neural network (CNN),

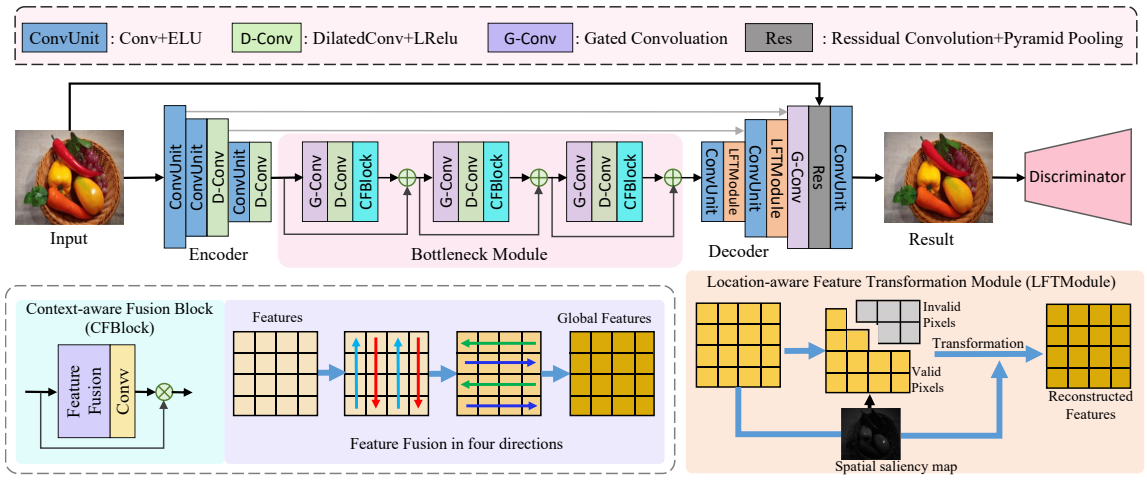

Figure 2: The framework of the proposed HighlightRNet. We first use an encoder to extract features. Then, we introduce a context-aware fusion block (CFBlock) in the bottleneck layer to learn global contextual information. Next, we embed two location-aware feature transformation modules (LFTModule) into the decoder, aiding in the reconstruction of high-quality highlight removal results with a consistent appearance.

which automatically and consistently removes specular highlights from a single image by generating its diffuse component. Muhammad *et al.* [20] introduced Spec-Net, which took an intensity channel as input to remove high-intensity specularity from low chromaticity images. They also proposed Spec-CGAN, which input an RGB image to produce a diffuse image. Wu *et al.* [29] presented a novel GAN for specular highlight removal with the guidance of the detected specular reflection information. Fu *et al.* [6] developed a multi-task network for joint highlight detection and removal based on a new specular highlight image formation model. These methods can handle small size as well as weak highlights, but they perform poorly for others and often exhibit color or texture distortion. More recently, Fu *et al.* [7] proposed a three-stage specular highlight removal network, which first decomposed the input image into the albedo, shading, and specular residue components. Such treatment may cause the error accumulation and reduce the performance of the subsequent highlight removal as intrinsic decomposition is also a difficult task.

3 NSH DATASET CONSTRUCTION

There are several image specular highlight datasets available, such as, SHIQ [6], PSD [29], and SSHR [7]. Table 1 summarizes the general information of the datasets. However, they still have some limitations:

- **SHIQ dataset:** The highlight-free images in SHIQ are computationally synthesized, with feature differences from the real-world images. In addition, this dataset lacks images with highlights caused by color illumination.
- **PSD dataset:** The variety of images is small and the background is simple. Some specular-free images have thin highlight residual. Also, the image pairs have misalignments and brightness variation in non-highlight regions.
- **SSHR dataset:** The images are rendered in software to simulate real images that have simple textures . The backgrounds in the images are blank and filled with black color, and the visual effects are lacking in realism.

In summary, the existing specular highlight datasets are still imperfect. To address this problem, we build an image-capturing system and construct a new and high-quality large-scale specular highlight dataset for image highlight removal. Our dataset is constructed on real scenes, and our image pairs have consistent brightness in non-highlight regions without misalignment.

Table 1: Image specular highlight datasets.

Dataset	Amount	Content of Images	DataType
SHIQ	16K	Specular/Specular-free /Specular mask	Synthetic
PSD	11.7K	Specular/Specular-free	Real
SSHR	130K	Specular/Specular-free /Albedo/Shading/Tone correction/Specular residue	Synthetic
Our NSH	30K	Specular/Specular-free	Real

3.1 Image-capturing System

The common light source in the real world is natural light, which is unpolarized light. Existing techniques [21, 29] often use cross polarizers to capture specular highlight images. In a strict laboratory environment [32], they convert a light source to linearly polarized light by adding a linear polarizer in front of the light source, as shown in Figure 3(a). When linearly polarized light strikes an object, it produces linearly polarized specular reflection and unpolarized diffuse reflection [2, 21]. As the two reflection lights pass through a linear polarizer, the observed image I can be represented as a linear combination of a constant diffuse reflection component I_d and a specular reflection component I_s, where I_s is modulated according to the polarization of the filter [27]. Based on the dichromatic

reflection model [22], the observed image I can be expressed as:

$$I = \frac{1}{2} I_d + I_s \cos^2 \phi \,, \tag{1}$$

where ϕ is a special angle between the two polarizers, as shown in Figure 3(a).

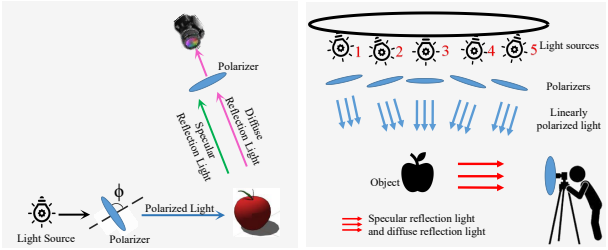

(a) Image capture with one light (b) Image capture with multiple lights

Figure 3: Specular highlight image capturing procedure. ϕ in (a) is a special angle between the two polarizers.

When capturing highlight images, we usually place a polarizer in front of both the camera and the light source. To prevent camera shake, we fix the polarizer in front of the camera, and rotate the polarizer in front of the light source to get the observed image. Wu *et al.* [29] use this strategy to construct PSD dataset. They capture the specular highlight image with $\phi = 0$ and get the corresponding diffuse image with $\phi = \frac{\pi}{2}$:

$$I = \begin{cases} \frac{1}{2} I_d + I_s, & \phi = 0 \\ \frac{1}{2} I_d, & \phi = \frac{\pi}{2} \end{cases} . \tag{2}$$

As we know, objects are basically non-Lambertian. When the linearly polarized light source strikes the object, the object's surface is usually divided into the highlight regions and the non-highlight regions. While $\phi = \frac{\pi}{2}$, linear specular reflections are filtered out, resulting in significant brightness variations in non-highlight regions for the image pairs. As shown the first heat map in Figure 4, the image pair from PSD has significant brightness variations in non-highlight regions. To solve this problem, we add the number of light sources to increase the diffuse reflection components, as shown in Figure 3(b). The superposition of light reflection components is a very complex process, and here we view the process as a linear one. Assuming there are n light sources in the environment, the observed image can indicate that,

$$I = \frac{1}{2} I_{d_1} + \cdots + \frac{1}{2} I_{d_n} + I_{s_1} \cos^2 \phi_1 + \cdots + I_{s_n} \cos^2 \phi_n \,, \tag{3}$$

where I_{d_i} and I_{s_i} are the diffuse reflection component and the specular reflection component produced by the i-th light source, and $i \in \{1, \cdots, n\}$. ϕ_i is the special angle between the two polarizers in front of the i-th light source and the camera.

Assuming the light sources have the same intensity, they have the same diffuse reflection component I_d and specular reflection component I_s. Thus, Eq. 3 can be rewritten as,

$$I = \frac{n}{2} I_d + \sum_{i=1}^{n} I_s \cos^2 \phi_i \,. \tag{4}$$

(a) Highlight image (b) Highlight-free image (c) Heat map

Figure 4: Comparison between the PSD and our NSH datasets. The image pair in the first row is from PSD, and the second row is from our NSH. The heat maps (c) highlight the differences between the highlight and highlight-free images. The heat map from our NSH consistently displays smaller values in non-highlight regions, indicating superior image pairs.

To obtain the image pair, we set $\phi_k = 0$ for the k-th light source, and the special angles of the other light sources are set to $\frac{\pi}{2}$. Then, the image pair is that,

$$I = \begin{cases} \frac{n}{2} I_d + I_s, & \phi_k = 0, \phi_j = \frac{\pi}{2}, j \in \{1, \cdots, n\} \wedge j \neq k \\ \frac{n}{2} I_d, & \phi_i = \frac{\pi}{2}, i \in \{1, \cdots, n\} \,. \end{cases} \tag{5}$$

Given sufficient light sources, the diffuse reflection components tend to infinity, and the effect of specular reflections on non-highlight regions is relatively small. At this time, if the specular reflections are filtered out, the brightness in the non-highlight regions will not change significantly. As shown in the heat maps in Figure 4, our image pairs remain unchanged from each other in non-highlight regions. Furthermore, we use a tripod to fix the camera and use a wireless trigger to control the capturing procedure of the image, avoiding camera shake and misalignment in the image pair due to manual camera manipulation.

To obtain a high-quality real-world dataset for image specular highlight removal, we built a simple yet effective image-capturing system, which consists of five light sources and a Conon 6D Mark II camera in a lighting-controlled environment, as shown in Figure 5(a, b). Note that, our image-capturing system is a movable device. We can move it to the desired environment for image capturing, both indoors and outdoors.

3.2 Dataset Collection

Our image collection process mainly includes the following four steps: 1) we place the image-capturing device in the desired environment; 2) we fix a rotatable polarizer in front of each light source and the camera; 3) we adjust the illumination direction and place an object in the intersection area of beams; 4) the image pair is captured by controlling the location of the light source and the polarizer. Specifically, according to Eq. 5, we first set all the light source's polarizers with $\phi = \pi/2$ to obtain a diffuse image (highlight-free image). Then, we rotate the polarizer of one light source with $\phi = 0$ to obtain a specular highlight image.

Repeating this process, we finally collect 30K image pairs from 3350 different scenes featuring a wide variety of materials that can easily produce highlights in daily life. Each image pair contains a highlight image and a corresponding highlight-free image. These

images are divided into three parts: 22K pairs for training, 6K for testing, and 2K for validation. Figure 5(c) presents some highlight and highlight-free image pairs in our NSH.

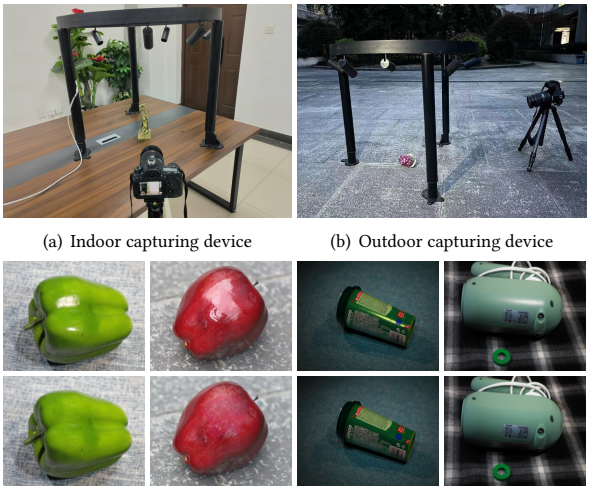

(a) Indoor capturing device (b) Outdoor capturing device

(c) Illustration of several captured image pairs in our NSH

Figure 5: Our image-capturing system and the captured image pairs. The top row in (c) is highlight images, and the bottom is corresponding highlight-free images (ground-truth).

4 PROPOSED METHOD

We propose an image specular highlight removal network called HighlightRNet, which leverages valid pixels in the image to reconstruct the highlight-free image. To better recognize the valid pixels, we first introduce a context-aware fusion block (CFBlock) to learn global contextual information in four different directions. Then, we propose a location-aware feature transformation module (LFTModule) to reconstruct features using valid pixels as referents.

Our HighlightRNet is an encoder-decoder structure stacked with a discriminator, as shown in Figure 2. The encoder employs a ConvUnit and two ConvUnit+D-Conv to extract features from the image. Each ConvUnit comprises a convolution operation followed by a LRelu function, while D-Conv represents a dilated convolution with a LRelu function. The bottleneck module consists of three fusion blocks, and each fusion block applies a gated convolution and a D-Conv alongside a CFBlock. There is a residual connection between two neighboring fusion blocks. The decoder employs two ConvUnit+LFTModule layers, followed by a gated convolution, a residual module, and a ConvUnit to reconstruct the highlight-free images.

Our discriminator is a binary classifier [13] to determine whether the predicted result is real or fake. It consists of six Conv+BN+ReLu layers and a fully connected layer. The final fully connected layer employs a sigmoid function to output the actual probability of the image.

4.1 Context-aware Fusion Block

The convolution operations typically operate in localized regions, which can prevent extracting global contextual features. For tasks like specular highlight removal, these localization-based convolutions may not capture contextual associations over longer distances, leading to color or texture distortion in the results. To address this issue, we introduce a context-aware fusion block (CFBlock) to learn and fuse contextual information in four different directions, enabling more effective utilization of global information.

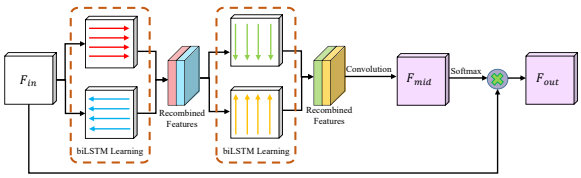

Figure 6: The network for our context-aware fusion block (CFBlock).

Figure 6 illustrates the architecture of the proposed CFBlock. Initially, we split the input features $F_{in} \in \mathbb{R}^{H\times W\times C}$ along the height dimension, where H, W and C are height, width and number of channels, respectively. We then employ bidirectional LSTM (biLSTM) [9] to learn the split features leftward and rightward pixel-by-pixel, enabling each pixel to retain its left and right contexts. Following biLSTM processing, we recombine the learned features. Subsequently, the combined features are split along the width dimension, and we conduct upward and downward pixel-by-pixel learning on the split features using biLSTM. After that, we recombine the learned features to obtain a new feature map $F_{context}$. By alternately scanning horizontally and vertically, our CFBlock effectively fuses contextual features in four directions and passes them from each pixel to the others, facilitating the perception of global contextual information.

Next, we apply a convolution to transform $F_{context}$ to $F_{mid} \in \mathbb{R}^{H\times W\times Z}$, where $Z = H\times W$. Consequently, we can obtain a feature vector f for each pixel. We then perform a softmax operation to normalize f along the channel dimension and obtain the contextual attention weights λ, which is that:

$$\lambda_i = \frac{exp(f_i)}{\sum_{j=1}^{Z} exp(f_j)}, \tag{6}$$

where $i \in \{1, \cdots, Z\}$, and $\lambda \in \mathbb{R}^Z$.

Finally, we perform matrix multiplication of F_{in} and λ to construct the global contextual features F_{out}:

$$F_{out} = \sum_{i=1}^{Z} \lambda_i F_{in}. \tag{7}$$

4.2 Location-aware Feature Transformation Module

Typically, the decoder utilizes all computed features to reconstruct the highlight-free image. However, it's crucial to note that regions with strong specular highlights are corrupted, and pixels in these regions are invalid for specular highlight removal. Processing all features uniformly can introduce invalid or biased convolution of pixels, potentially leading to errors in feature computation and the generation of undesirable removal results, such as color distortion and highlight residual.

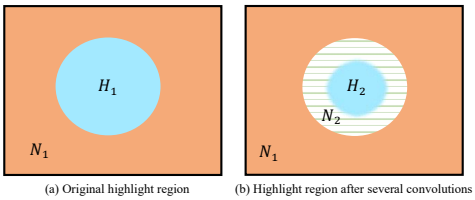

Figure 7: The specular highlight region. N_1 and H_1 denote the original non-highlight region and the highlight region. After passing through several convolutions, highlights in N_2 have been removed, and N_2 can be considered as a non-highlight region. H_2 is the remaining highlight region.

Furthermore, after several convolution operations, the specular highlights are gradually removed, as shown in Figure 7, indicating that the specular highlight regions are dynamically changing during the decoding process. The repaired contents, such as N_2 in Figure 7(b), can also be considered as valid pixels for the restoration of the remaining highlighted regions.

Based on the preceding analysis, we introduce a location-aware feature transformation module (LFTModule), which reconstructs features using valid pixels as references. LFTModule utilizes the spatial relationship of input features to learn a spatial saliency map, which represents the distribution and intensity of the highlights at the current layer. Larger values in the spatial saliency map indicate stronger highlights at the corresponding positions. The stronger the highlight, the higher the probability that the pixel is invalid. With the spatial saliency map, we can identify which pixels are valid for feature reconstruction. Consequently, we can selectively manipulate the image features using valid pixels as referents, thereby avoiding information error caused by uniform feature processing and boosting satisfactory highlight-free results without color distortion and highlight residual.

Figure 8 illustrates the pipeline of our LFTModule. For the input feature $F_{de} \in \mathbb{R}^{H\times W\times C}$, we first apply max-pooling and global average pooling along the channel axis to obtain efficient feature descriptor. We then integrate the results of these two pooling operations and perform a convolution operation followed by a sigmoid function to compute a spatial saliency map $A \in \mathbb{R}^{H\times W\times 1}$. We can utilize the spatial saliency map to identify valid pixels based on a threshold t. If $A(h,w) < t$, we consider pixel (h,w) to be a valid pixel, where (h,w) is an index of (H,W) axis. Otherwise, we consider this pixel to be located in a strong highlight region and thus invalid for specular highlight removal. In our experiments, we set $t = 0.5$.

Next, we utilize the valid pixels to normalize the input features and result in feature M_1. The normalization is region-based, performed separately for the valid pixel region and the invalid pixel region. This process can address the mean and variance shifts caused by invalid pixels. Since the spatial saliency map A contains global spatial information, we use convolution operation for A to learn a global representation. We perform convolution operation on A respectively to obtain two parameters, γ and β. We then use γ and β as affine parameters to perform pixel-wise affine transformation on M_1, obtaining the reconstructed features. With this affine transformation, our LFTModule promotes consistent-looking results for the highlight regions with the surrounding environment.

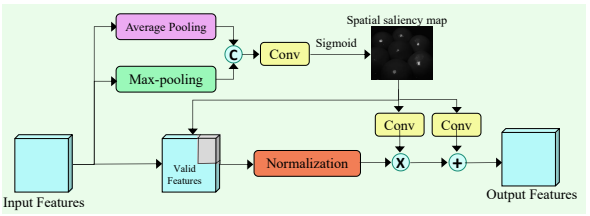

Figure 8: The network for our location-aware feature transformation module (LFTModule).

4.3 Loss Functions

The loss function for training our HightlightRNet contains three components: color consistency loss $\mathcal{L}_{color}$, texture consistency loss $\mathcal{L}_{texture}$ and adversarial loss $\mathcal{L}_{adv}$.

Color consistency loss is used to suppress the color distortion during the reconstruction process. It is calculated using the mean squared errors (MSE) between the predicted highlight removal result I_{free} and the ground-truth image I_{gt}, as follows:

$$\mathcal{L}_{color} = \|I_{free} - I_{gt}\|_2^2 .$$

Texture consistency loss aims to preserve image structure using the gradient information in the image. It can prevent the generation of blurry results. Our texture consistency loss $\mathcal{L}_{texture}$ is calculated as,

$$\mathcal{L}_{texture} = \|\nabla_x I_{free} - \nabla_x I_{gt}\|_1 + \|\nabla_y I_{free} - \nabla_y I_{gt}\|_1 , \quad (8)$$

where ∇_x represents the gradient along the x-direction and ∇_y represents the gradient along the y-direction.

Adversarial loss. We employ relativistic average adversarial loss [13] to implement our adversarial loss $\mathcal{L}_{adv}$, which is described as:

$$\begin{aligned}\mathcal{L}_{adv} = 0.5 \cdot (&BCE(\sigma(D(I_{free}) - D(I_{gt})), y') \\ &+BCE(\sigma(D(I_{free}) - D(I_{gt})), y)) ,\end{aligned} \quad (9)$$

where σ is the sigmoid function and $BCE(*)$ measures the binary cross entropy. (y', y) is set as $(1, 0)$ for the generator and $(0, 1)$ for the discriminator, respectively. D is our discriminator.

In summary, the total loss for our method is written as:

$$\mathcal{L} = \lambda_1 \mathcal{L}_{color} + \lambda_2 \mathcal{L}_{texture} + \lambda_3 \mathcal{L}_{adv} , \quad (10)$$

where λ_1, λ_2 and λ_3 are the weighting parameters. In our experiments, we empirically set $\lambda_1 = 1.0$, $\lambda_2 = 1$, and $\lambda_3 = 0.01$.

5 EXPERIMENTS

5.1 Implementation Details

Our network is implemented in PyTorch. We utilize the Adam optimizer [16] to train our HightlightRNet on an NVIDIA GeForce RTX 2080 Ti GPR for 80 epochs, with a batch size of 8. The initial learning rate is set to 2×10^{-4} and is decayed by a factor of $1/2$ every 10 epochs, until it reaches a value lower than 10^{-5}.

5.2 Datasets and Evaluation Metrics

We evaluate the method on four datasets, including our NSH, SHIQ [6], SSHR [7] and PSD [29]. We employ structural similarity index (SSIM) and peak signal-to-noise ratio (PSNR), to quantitatively evaluate the performance of our method.

Table 2: Quantitative comparisons of highlight removal on NSH, SHIQ, PSD and SSHR datasets. ↑ means the larger the better. The best results are marked in bold.

Methods	Venue/Year	NSH		SHIQ		PSD		SSHR	
		SSIM↑	PSNR↑	SSIM↑	PSNR↑	SSIM↑	PSNR↑	SSIM↑	PSNR↑
Yamamoto *et al.* [30]	MTA/2019	0.683	14.651	0.820	20.513	0.697	19.897	0.844	22.403
Shen *et al.* [25]	AO/2012	0.872	20.638	0.811	20.621	0.732	19.438	0.891	23.072
Yang *et al.* [33]	CV/2010	0.633	19.651	0.776	17.323	0.753	15.942	0.864	23.717
Wu *et al.* [29]	TMM/2021	0.899	29.921	0.875	28.637	0.910	29.153	0.923	27.271
Fu *et al.* [6]	CVPR/2021	0.903	28.893	0.899	29.732	0.870	27.846	0.914	26.131
Fu *et al.* [7]	ICCV/2023	0.901	26.211	0.917	27.475	0.897	26.274	0.937	29.014
HighlightRNet	ACMMM/2024	**0.942**	**30.672**	**0.930**	**30.231**	**0.922**	**29.787**	**0.956**	**30.066**

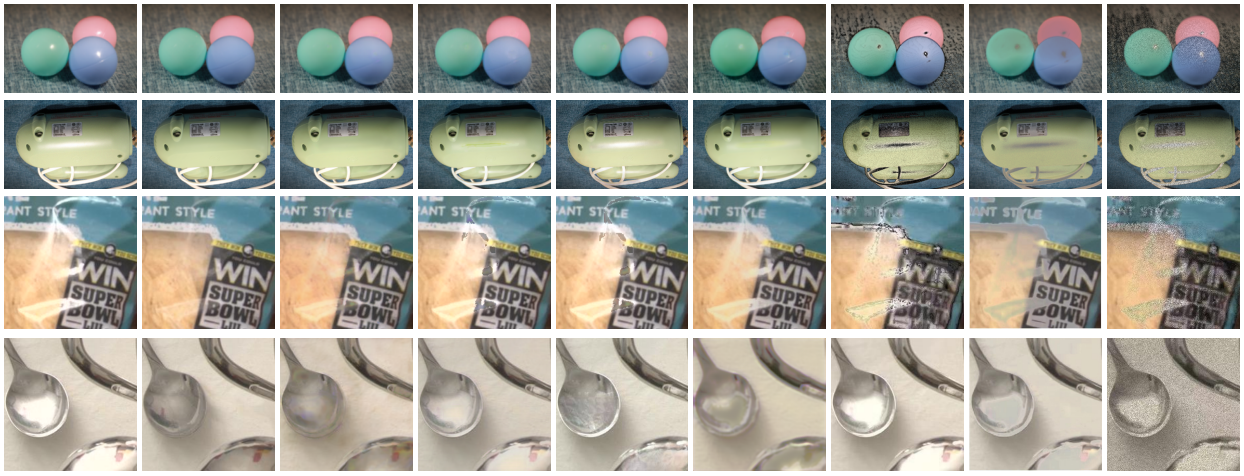

(a) Input (b) GT (c) Our results (d) Fu [7] (e) Fu [6] (f) Wu [29] (g) Yang [33] (h) Shen [25] (i) Yamato [30]

Figure 9: Visual comparison of our method against state-of-the-art highlight removal methods. Compared with other results, our method produce satisfactory results without color distortion and highlight residual.

5.3 Comparison with State-of-The-Art Methods

To verify the effectiveness of our method, we compare our method with three learning-based methods [6, 7, 29] and three traditional methods [25, 30, 33]. For a fair comparison, we directly use the codes provided by the authors with recommended parameter settings and retrain the learning-based methods on the same hardware. To train and evaluate method of Fu *et al.* [7] on the four datasets, we modify their method and estimate the highlight-free and highlight residue instead of the original albedo and shading at the first stage.

Quantitative Comparison. Table 2 presents the quantitative comparisons on three datasets. From the table, we can observe that, our method achieves larger SSIM and PSNR scores on all datasets, indicating the better performance of our method compared to existing state-of-the-art methods.

Visual Comparison. Figure 9 presents some visual highlight removal results to further demonstrate the effectiveness of our method. With inaccurate shadow detection results, Fu *et al.* [6] and Wu *et al.* [29] may produce undesirable results with highlight residual, as shown in Figure 9(e, f). Without adequate information to guide, Fu *et al.* [7] may result in color distortion or incomplete removal of highlights, as shown in Figure 9(d). Due to the lack of ability to capture high-level semantic information, the three traditional methods do not make good use of non-highlight pixels to restore the highlight regions, which usually result in color or texture distortion. For example, Yang *et al.* [32] suffer from severe artifacts such as black blocks and color distortion, as shown in Figure 9(g). Shen *et al.* [25] often result in texture loss, as shown in Figure 9(h). Yamamoto *et al.* [30] also suffer from black blocks and color distortion, as shown in Figure 9(i). Comparatively, our method effectively removes highlight and recovers the content in the image without artifacts, which are closer to the ground truth images, as shown in Figure 9(b) and Figure 9(c).

To further verify the robustness and generalization ability of our HightlightRNet, Figure 12 presents some other highlight removal results for real-world natural images captured by smartphones or downloaded from the internet. Even for images with complex lighting conditions and object textures, our method is able to achieve satisfactory results, as shown in Figure 12.

5.4 Ablation Study

We performed a series of experiments to validate the effectiveness of our method and the superiority of our dataset.

Effectiveness of the network. To demonstrate the effectiveness of our HightlightRNet, we compare our network with four variants to assess the impact of each component. The variants are (1)

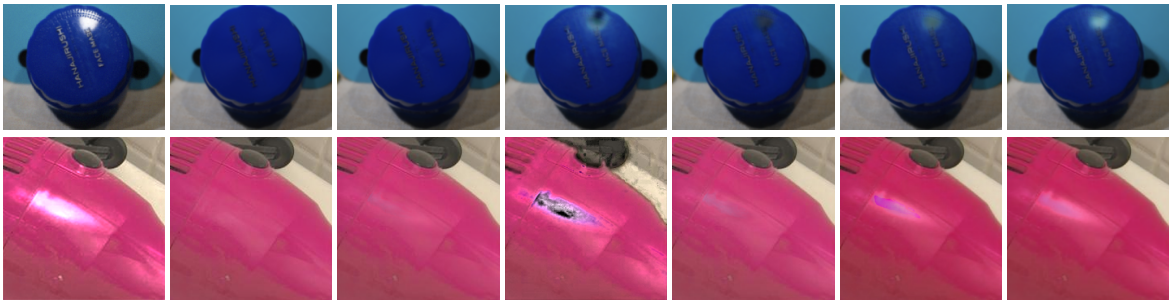

(a) Input (b) GT (c) Our results (d) Results of M_1 (e) Results of M_2 (f) Results of M_3 (g) Results of M_4

Figure 10: Visual comparison for ablation study. Compared with other variants, our HighlightRNet can produce more natural results.

Table 3: Quantitative results of ablation study on NSH, SHIQ and PSD. The best results are marked in bold. ↑ means the larger the better.

Methods	NSH		SHIQ		PSD	
	SSIM↑	PSNR↑	SSIM↑	PSNR↑	SSIM↑	PSNR↑
M_1	0.836	25.534	0.824	25.637	0.838	25.347
M_2	0.901	26.941	0.877	26.554	0.873	25.199
M_3	0.888	28.431	0.852	26.978	0.847	27.201
M_4	0.876	28.433	0.851	27.207	0.836	26.954
HighlightRNet	**0.942**	**30.672**	**0.930**	**30.231**	**0.922**	**29.787**

(a) Input (b) Our result (c) Input (d) Our result

Figure 11: Highlight removal results for real-world natural highlight images with complex scenes.

M_1: remove CFBlock in HightlightRNet; (2) M_2: replace LFTModule with batchNorm; (3) M_3: remove $\mathcal{L}_{texture}$ for training HightlightRNet; and (4) M_4: remove $\mathcal{L}_{adv}$ for training HightlightRNet. We train the variants on NSH. Table 3 summarizes the evaluated results on three datasets. From the table, we can observe: (1) our HightlightRNet with all components gets the best results; (2) the proposed CFBlock and LFTModule can help improve the performance of the network, and the combination leads to the best performance; and (3) the loss functions $\mathcal{L}_{texture}$ and $\mathcal{L}_{adv}$ are necessary to ensure the high-quality highlight removal results. We also provide the visualization in Figure 10, from which we can see that results produced by our HightlightRNet look more realistic with fewer artifacts.

Superiority of NSH dataset. To validate the superiority of our NSH dataset, we train our HighlightRNet using four datasets: SHIQ, PSD, SSHR, and our NSH datasets. Table 4 summarizes the evaluation results on NSH dataset. It is evident from the table that the model trained with our NSH dataset outperforms the models trained with the other datasets, highlighting the superiority of our NSH dataset.

Table 4: Ablation study about NSH dataset. The quantitative results are evaluated on NSH. The best results are marked in bold.

Methods	SSIM ↑	PSNR↑
Training on SHIQ	0.824	23.662
Training on PSD	0.798	23.512
Training on SSHR	0.844	25.291
HighlightRNet training on NSH	**0.942**	**30.672**

Limitation. Our method can effectively remove specular highlight in the image. However, when the highlight is too strong and the area is large, it can mask a large amount of information, resulting in not-so-desirable recovery result.

Figure 12: Limitation. The left is the highlight image, and the right is the highlight removal result.

6 CONCLUSIONS

In this paper, we have proposed a new network called HighlightRNet for image specular highlight removal, which utilizes valid pixels in non-highlight regions to reconstruct highlight-free image. Particularly, we introduced a context-aware fusion block (CFBlock) to learn global contextual information in four directions. We also proposed a location-aware feature transformation module (LFTModule) to adaptively learn the valid pixels for feature reconstruction. Furthermore, we have constructed a new real-work highlight dataset for specular highlight removal. Experiments qualitatively and quantitatively demonstrate the superiority of our method over the state-of-the-art methods.

ACKNOWLEDGMENTS

This work is partially supported by the National Natural Science Foundation of China (No.62372336, No.61902286, No.61972298), Wuhan UniversityHuawei GeoInformatices Innovation Lab and Nature Science Foundation of Hubei Province (No.2023AFB615). Thank Xiaoxiao Long for his insightful suggestions on the paper.

REFERENCES

[1] Yasuhiro Akashi and Takayuki Okatani. 2014. Separation of reflection components by sparse non-negative matrix factorization. In *Asian Conference on Computer Vision*. Springer, 611–625.

[2] Max Born and Emil Wolf. 2013. *Principles of optics: electromagnetic theory of propagation, interference and diffraction of light*. Elsevier.

[3] Daniele Di Mauro, Antonino Furnari, Giuseppe Patanè, Sebastiano Battiato, and Giovanni Maria Farinella. 2020. SceneAdapt: Scene-based domain adaptation for semantic segmentation using adversarial learning. *Pattern Recognition Letters* 136 (2020), 175–182.

[4] Gang Fu, Qing Zhang, Qifeng Lin, Lei Zhu, and Chunxia Xiao. 2020. Learning to Detect Specular Highlights from Real-world Images. In *ACM International Conference on Multimedia*.

[5] Gang Fu, Qing Zhang, and Chunxia Xiao. 2024. Towards High-Resolution Specular Highlight Detection. *International Journal of Computer Vision* 132, 1 (2024), 95–117.

[6] Gang Fu, Qing Zhang, Lei Zhu, Ping Li, and Chunxia Xiao. 2021. A multi-task network for joint specular highlight detection and removal. In *Proceedings of the IEEE/CVF Conference on Computer Vision and Pattern Recognition*. 7752–7761.

[7] Gang Fu, Qing Zhang, Lei Zhu, Chunxia Xiao, and Ping Li. 2023. Towards High-Quality Specular Highlight Removal by Leveraging Large-Scale Synthetic Data. In *Proceedings of the IEEE/CVF International Conference on Computer Vision (ICCV)*. 12857–12865.

[8] Junyu Gao, Tianzhu Zhang, and Changsheng Xu. 2019. Graph convolutional tracking. In *Proceedings of the IEEE/CVF Conference on Computer Vision and Pattern Recognition*. 4649–4659.

[9] Alex Graves, Navdeep Jaitly, and Abdel-rahman Mohamed. 2013. Hybrid speech recognition with deep bidirectional LSTM. In *2013 IEEE workshop on automatic speech recognition and understanding*. IEEE, 273–278.

[10] Xiaojie Guo, Xiaochun Cao, and Yi Ma. 2014. Robust separation of reflection from multiple images. In *Proceedings of the IEEE conference on computer vision and pattern recognition*. 2187–2194.

[11] Guangwei Hu, Yuanfeng Zheng, Haoran Yan, Guang Hua, and Yuchen Yan. 2022. Mask-guided cycle-GAN for specular highlight removal. *Pattern Recognition Letters* 161 (2022), 108–114.

[12] Zhaoyangfan Huang, Kun Hu, and Xingjun Wang. 2022. M2-Net: multi-stages specular highlight detection and removal in multi-scenes. *arXiv preprint arXiv:2207.09965* (2022).

[13] Alexia Jolicoeur-Martineau. 2018. The relativistic discriminator: a key element missing from standard GAN. *arXiv preprint arXiv:1807.00734* (2018).

[14] Hyeongwoo Kim, Hailin Jin, Sunil Hadap, and Inso Kweon. 2013. Specular reflection separation using dark channel prior. In *Proceedings of the IEEE conference on computer vision and pattern recognition*. 1460–1467.

[15] Seung-Wook Kim, Hyong-Keun Kook, Jee-Young Sun, Mun-Cheon Kang, and Sung-Jea Ko. 2018. Parallel feature pyramid network for object detection. In *Proceedings of the European Conference on Computer Vision (ECCV)*. 234–250.

[16] Diederik P Kingma and Jimmy Ba. 2014. Adam: A method for stochastic optimization. *arXiv preprint arXiv:1412.6980* (2014).

[17] Gudrun J Klinker, Steven A Shafer, and Takeo Kanade. 1988. The measurement of highlights in color images. *International Journal of Computer Vision* 2, 1 (1988), 7–32.

[18] John Lin, Mohamed El Amine Seddik, Mohamed Tamaazousti, Youssef Tamaazousti, and Adrien Bartoli. 2019. Deep multi-class adversarial specularity removal. In *Scandinavian Conference on Image Analysis*. Springer, 3–15.

[19] Stephen Lin, Yuanzhen Li, Sing Bing Kang, Xin Tong, and Heung-Yeung Shum. 2002. Diffuse-specular separation and depth recovery from image sequences. In *European conference on computer vision*. Springer, 210–224.

[20] Siraj Muhammad, Matthew N Dailey, Muhammad Farooq, Muhammad F Majeed, and Mongkol Ekpanyapong. 2020. Spec-Net and Spec-CGAN: Deep learning models for specularity removal from faces. *Image and Vision Computing* 93 (2020), 103823.

[21] Shree K Nayar, Xi-Sheng Fang, and Terrance Boult. 1997. Separation of reflection components using color and polarization. *International Journal of Computer Vision* 21, 3 (1997), 163–186.

[22] S Shafer. 1992. Using Color to Separate Reflection Components. *Jones and Bartlett Publishers, Inc.* (1992).

[23] Steven A Shafer. 1985. Using color to separate reflection components. *Color Research & Application* 10, 4 (1985), 210–218.

[24] Hui-Liang Shen, Hong-Gang Zhang, Si-Jie Shao, and John H Xin. 2008. Chromaticity-based separation of reflection components in a single image. *Pattern Recognition* 41, 8 (2008), 2461–2469.

[25] Hui-Liang Shen and Zhi-Huan Zheng. 2013. Real-time highlight removal using intensity ratio. *Applied optics* 52, 19 (2013), 4483–4493.

[26] Jinli Suo, Dongsheng An, Xiangyang Ji, Haoqian Wang, and Qionghai Dai. 2016. Fast and high quality highlight removal from a single image. *IEEE Transactions on Image Processing* 25, 11 (2016), 5441–5454.

[27] Laurent Valentin Jospin, Gilles Baechler, and Adam Scholefield. 2018. Embedded polarizing filters to separate diffuse and specular reflection. *arXiv e-prints* (2018), arXiv–1811.

[28] Xing Wei, Xiaobin Xu, Jiawei Zhang, and Yihong Gong. 2018. Specular highlight reduction with known surface geometry. *Computer Vision and Image Understanding* 168 (2018), 132–144.

[29] Zhongqi Wu, Chuanqing Zhuang, Jian Shi, Jianwei Guo, Jun Xiao, Xiaopeng Zhang, and Dong-Ming Yan. 2021. Single-image specular highlight removal via real-world dataset construction. *IEEE Transactions on Multimedia* 24 (2021), 3782–3793.

[30] Takahisa Yamamoto and Atsushi Nakazawa. 2019. General improvement method of specular component separation using high-emphasis filter and similarity function. *ITE Transactions on Media Technology and Applications* 7, 2 (2019), 92–102.

[31] Jianwei Yang, Lixing Liu, and Stan Li. 2013. Separating specular and diffuse reflection components in the HSI color space. In *Proceedings of the IEEE International Conference on Computer Vision Workshops*. 891–898.

[32] Qingxiong Yang, Jinhui Tang, and Narendra Ahuja. 2014. Efficient and robust specular highlight removal. *IEEE transactions on pattern analysis and machine intelligence* 37, 6 (2014), 1304–1311.

[33] Qingxiong Yang, Shengnan Wang, and Narendra Ahuja. 2010. Real-time specular highlight removal using bilateral filtering. In *European conference on computer vision*. Springer, 87–100.

[34] Ling Zhang, Chengjiang Long, Xiaolong Zhang, and Chunxia Xiao. 2023. Exploiting Residual and Illumination with GANs for Shadow Detection and Shadow Removal. *ACM transactions on multimedia computing communications and applications* 19, 3 (2023), 120.1–120.22.

[35] Wuming Zhang, Xi Zhao, Jean-Marie Morvan, and Liming Chen. 2018. Improving shadow suppression for illumination robust face recognition. *IEEE transactions on pattern analysis and machine intelligence* 41, 3 (2018), 611–624.